Cartilage tissue engineering using differentiated and purified induced pluripotent stem cells

Brian O. Diekman[a,b], Nicolas Christoforou[b,c], Vincent P. Willard[a], Haosi Sun[a,b], Johannah Sanchez-Adams[a], Kam W. Leong[b], and Farshid Guilak[a,b,1]

[a]Department of Orthopaedic Surgery, Duke University Medical Center, Durham, NC 27710; [b]Department of Biomedical Engineering, Duke University, Durham, NC 27708; and [c]Biomedical Engineering Department, Khalifa University of Science Technology and Research, P.O. Box 127788, Abu Dhabi, United Arab Emirates

Edited* by Shu Chien, University of California at San Diego, La Jolla, CA, and approved October 4, 2012 (received for review June 21, 2012)

The development of regenerative therapies for cartilage injury has been greatly aided by recent advances in stem cell biology. Induced pluripotent stem cells (iPSCs) have the potential to provide an abundant cell source for tissue engineering, as well as generating patient-matched in vitro models to study genetic and environmental factors in cartilage repair and osteoarthritis. However, both cell therapy and modeling approaches require a purified and uniformly differentiated cell population to predictably recapitulate the physiological characteristics of cartilage. Here, iPSCs derived from adult mouse fibroblasts were chondrogenically differentiated and purified by type II collagen (Col2)-driven green fluorescent protein (GFP) expression. Col2 and aggrecan gene expression levels were significantly up-regulated in GFP+ cells compared with GFP− cells and decreased with monolayer expansion. An in vitro cartilage defect model was used to demonstrate integrative repair by GFP+ cells seeded in agarose, supporting their potential use in cartilage therapies. In chondrogenic pellet culture, cells synthesized cartilage-specific matrix as indicated by high levels of glycosaminoglycans and type II collagen and low levels of type I and type X collagen. The feasibility of cell expansion after initial differentiation was illustrated by homogenous matrix deposition in pellets from twice-passaged GFP+ cells. Finally, atomic force microscopy analysis showed increased microscale elastic moduli associated with collagen alignment at the periphery of pellets, mimicking zonal variation in native cartilage. This study demonstrates the potential use of iPSCs for cartilage defect repair and for creating tissue models of cartilage that can be matched to specific genetic backgrounds.

chondrocyte | bone morphogenetic proteins | transforming growth factor-beta | cartilage micromechanics | cartilage regeneration

Articular cartilage exhibits poor intrinsic capacity for repair, and focal cartilage defects often progress to osteoarthritis (OA) eventually requiring total joint replacement (1). Cartilage tissue engineering seeks to provide a biological replacement tissue, which requires an adequate cell source (2, 3). Although autologous chondrocytes have previously been used for the treatment of focal defects (4), their derivation requires additional surgical procedures leading to possible complications at the donor site (5). Adult stem cells are a promising alternative cell source due to their minimally invasive isolation and chondrogenic potential (6, 7), but these cells also have limitations. The percentage of mesenchymal stem cells (MSCs) in bone marrow is low (8), whereas the more abundant adipose-derived stem cells (ASCs) appear to have reduced chondrogenic potential under current differentiation protocols (9). Additionally, the yield of adult stem cells from patients most likely to require such cartilage therapies may be insufficient, as MSCs from older patients show lower proliferation rates in culture (10) and MSCs from patients with OA demonstrate reduced chondrogenic differentiation (11).

Induced pluripotent stem cells (iPSCs) have the capacity to overcome limitations associated with the current cell sources, primarily because large numbers of patient-matched cells with chondrogenic potential can be derived from a minimally invasively isolated starting cell population. As somatic cells that have been genetically reprogrammed to a pluripotent state, iPSCs demonstrate significant expansion potential while maintaining their multilineage differentiation capacity (12–14). In addition to cell-based therapeutic applications, iPSC technology can also provide patient-specific cell and tissue models for pathophysiological and pharmacological studies (15, 16). This characteristic also allows engineered cartilage constructs from specific mouse strains to be used for mechanistic investigation into the effects of specific genetic traits on cartilage development, repair, and OA.

One of the main challenges in using iPSCs for either therapeutic applications or in vitro modeling is the difficulty in achieving uniform differentiation to the cell type of interest (17). A non-uniform cell population not only limits the effectiveness of the therapy or model, but also increases the risk for undifferentiated cells contained in the population to contribute to teratoma formation (18). Previous work with mouse and human embryonic stem cells has demonstrated that chondrogenesis of pluripotent cells can be initiated by exposure to growth factors such as the bone morphogenetic proteins (BMPs) (19, 20) and transforming growth factor-beta (TGF-β) (21, 22). Chondrogenesis can be further enhanced by recapitulating features of mesenchymal condensation using 3D culture systems such as embryoid bodies (23), micromasses (24, 25), pellets (26), or scaffolds (27). These techniques have also been effective in initial studies with mouse and human iPSCs (28–31). However, the inability to differentiate every pluripotent cell toward the chondrogenic lineage has limited the potential to engineer a tissue with uniform cartilaginous matrix.

The goal of this study was to create tissue-engineered cartilage constructs from murine iPSCs by using a starting population of cells that were successfully predifferentiated toward the chondrogenic lineage. To accomplish this, we induced chondrogenic differentiation by treating micromass cultures with BMP-4 and used flow cytometry to sort cells expressing green fluorescent protein (GFP) under control of the chondrocyte-specific type II collagen (Col2) promoter/enhancer (32). In addition to biochemical and mechanical characterization of the tissue-engineered constructs, we examined the potential of differentiated and purified iPSCs to be used for functional cartilage repair using an in vitro cartilage defect model system.

Results

Somatic Cell Reprogramming into Induced Pluripotent Stem Cells. Successful reprogramming of tail fibroblasts from 8- to 10-wk-old mice through the forced overexpression of a core set of transcription factors (Oct4, Sox2, Klf4, and Myc) was verified by morphology, the presence of pluripotency markers, and the

Author contributions: B.O.D., N.C., V.P.W., K.W.L., and F.G. designed research; B.O.D., N.C., V.P.W., H.S., and J.S.-A. performed research; B.O.D., V.P.W., and J.S.-A. analyzed data; and B.O.D. and F.G. wrote the paper.

The authors declare no conflict of interest.

*This Direct Submission article had a prearranged editor.

[1]To whom correspondence should be addressed. E-mail: guilak@duke.edu.

This article contains supporting information online at www.pnas.org/lookup/suppl/doi:10.1073/pnas.1210422109/-/DCSupplemental.

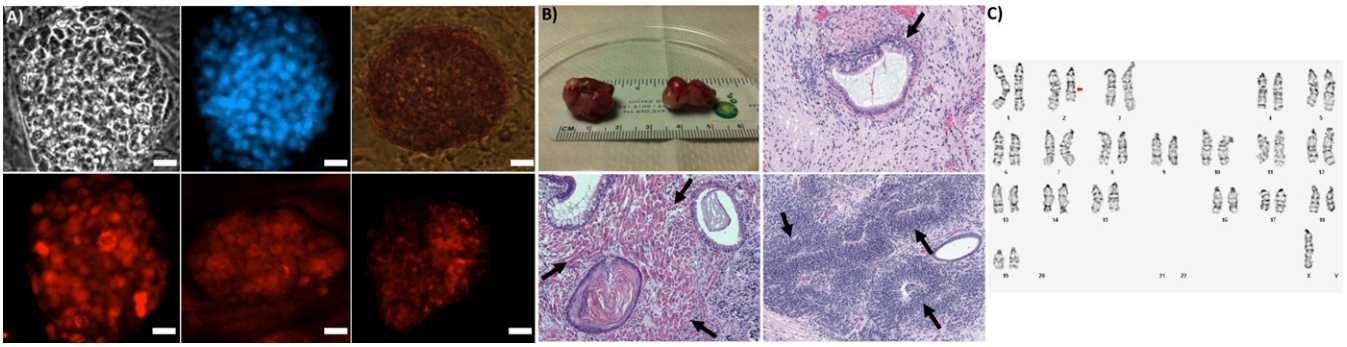

Fig. 1. Characterization of iPSCs. (*A*) Pluripotency markers (top left to right, bottom left to right; scale bars: 20 μm): bright field, DAPI, alkaline phosphatase, nanog, Oct4/Pou5f1, SSEA1. (*B*) Undifferentiated iPSCs formed teratomas (*Upper Left*) with endoderm (gland, *Upper Right*), mesoderm (muscle, *Lower Left*), and ectoderm (neural rosette, *Lower Right*). (*C*) Karyogram from G banding, arrow indicates deletion.

formation of teratomas. Cells formed rounded colonies on top of the feeder cells with morphology similar to that of embryonic stem cells (Fig. 1*A*). Cells stained positive for alkaline phosphatase, Nanog, Oct4/Pou5f1, and stage-specific embryonic antigen 1 (SSEA-1) (Fig. 1*A*). Pluripotency was confirmed by the formation of teratomas after injection of undifferentiated iPSCs in the kidney and testis of mice. The resulting teratomas included tissue types of all three germ layers, including gland tissue (endoderm), muscle (mesoderm), and neural rosettes (ectoderm) (Fig. 1*B*). The karyotype of the iPSCs was determined using G banding analysis, indicating an interstitial deletion from 2D to 2F3 in chromosome 2 and the loss of the Y sex chromosome (Fig. 1*C*).

Chondrogenically Differentiated Cells Can Be Identified and Isolated Based on Col2 Expression Driving GFP. The addition of BMP-4 and dexamethasone during days 3–5 of micromass culture initiated chondrogenic differentiation in a subset of the iPSCs. After 15 d of micromass culture, ~10% of cells expressed GFP under the control of the Col2 promoter/enhancer and flow cytometry was used to sort cells based on GFP expression (Fig. S1). Cells sorted for lack of GFP expression (hereafter termed GFP− cells) were spindle-shaped and negative for type II collagen by immunocytochemistry, whereas cells sorted for the positive expression of GFP (hereafter termed GFP+ cells) displayed a rounded phenotype and expressed type II collagen (Fig. S1). Quantitative RT-PCR analysis performed on cells immediately after sorting demonstrated an increase in the expression of chondrogenic genes in GFP+ compared with GFP− cells, including Col2, aggrecan (Acan), type X collagen (Col10), and Sox9, while displaying decreased expression of type I collagen (Col1) (Table S1). Both cell populations showed reduced gene expression of the pluripotency marker Nanog compared with undifferentiated iPSCs (Table S1).

Monolayer Expansion Alters Chondrogenic Gene Expression. Sorted cells retained distinct morphologies in monolayer culture, with GFP− cells remaining spindle-shaped and GFP+ cells remaining more rounded (Fig. 2*A*). In the presence of 10% (vol/vol) FBS and 4 ng/mL bFGF, both the GFP+ and GFP− cells showed extensive proliferation, with 2366-fold and 264-fold cumulative expansion over six passages, respectively (Fig. 2*B*). The chondrocyte-specific gene markers Col2 and Acan showed significantly higher gene expression levels in GFP+ compared with GFP− cell populations after either one or two passages. Expression of Col2 and Acan decreased with passaging in both GFP + and GFP− cells (Fig. 2*C*). The gene expression level of the early chondrocyte marker Sox9 was similar in GFP+ and GFP− cells and was generally stable over passaging, but decreased by passage 3 in GFP+ cells. The expression level of the hypertrophic chondrocyte marker Col10 was higher in the GFP+ cells during the first two passages; however, it increased with passaging in the GFP− cells but not in GFP+ cells. Col1 expression levels were higher in GFP− cells compared with GFP+ cells after the first passage. Col1 increased in GFP+ cells after an additional passage, but was stable with passaging in GFP− cells.

Enhanced GAG Synthesis in Pellets Formed from GFP+ Cells. Following monolayer expansion, cells were centrifuged to form pellets, which were subsequently cultured for 21 d in the presence of TGF-β3. As visualized by the diameter of central histological sections, pellet cultures from GFP+ cells were larger than those from GFP− cells, and the size of GFP+ pellets decreased with increased passaging (Fig. 3*A*). Safranin-O staining of sectioned pellets demonstrated robust production of glycosaminoglycans (GAGs) in pellets formed using GFP+ cells (Fig. 3*A*). In pellets formed using either passage 1 or passage 3 GFP+ cells, the central region of the pellet did not show uniform GAG production. However, pellets formed using passage 2 GFP+ cells exhibited rich GAG staining throughout the whole pellet. Safranin-O staining was confined to the outer regions of pellets formed using GFP− cells (Fig. 3*A*) and "unsorted" cells (Fig. S2). Quantification of GAG production supported the histology, as pellets from GFP+ cells had higher GAG production than corresponding pellets from GFP− cells at each passage (Fig. 3*B*). Although total

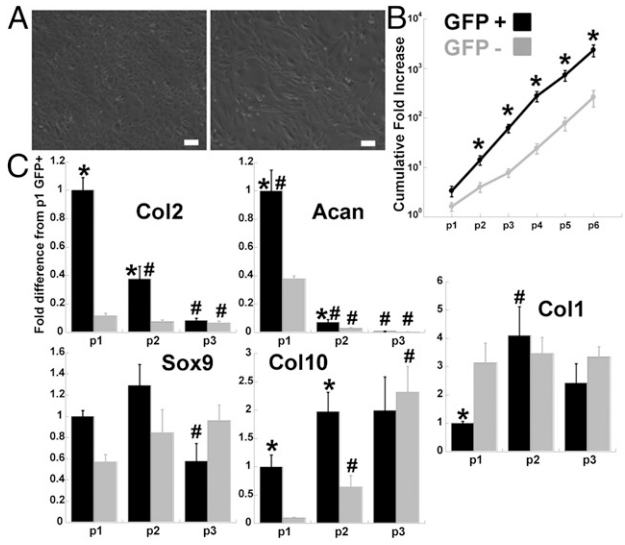

Fig. 2. Monolayer expansion of sorted cells. (*A*) Passage 2 cells after sorting for GFP+ (left) or GFP− (right). (Scale bar: 100 μm.) (*B*) Cumulative fold increase in cell number (log scale). Asterisk indicates $P < 0.05$ to GFP− of same passage, $n \geq 3$ per group, mean ± SEM. (*C*) RT-PCR. Fold increase normalized to passage 1 GFP+ cells, asterisk indicates $P < 0.05$ to GFP− of same passage and pound indicates $P < 0.05$ to passage 1 of own cell type, $n \geq 3$ per group, mean ± SEM.

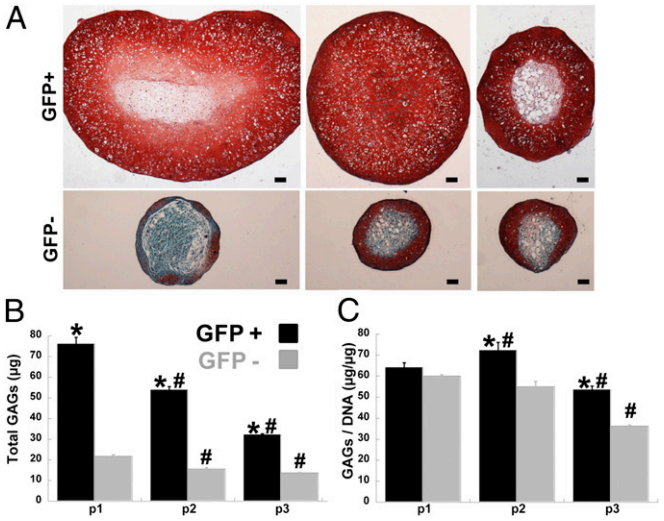

Fig. 3. Glycosaminoglycans (GAGs) production. (*A*) Safranin-O/Fast-Green/Hematoxylin stained section from pellets of GFP+ or GFP− cells passaged once (*Left*), twice (*Center*), or three times (*Right*) after sorting. (Scale bar: 100 μm.) (*B* and *C*) Total GAGs per pellet (*B*) andGAGs per DNA by DMB assay (*C*), asterisk indicates $P < 0.05$ to GFP− of same passage and pound indicates $P < 0.05$ to passage 1 of own cell type, $n \geq 4$ per group, mean ± SEM.

GAG content was higher in pellets from passage 1 GFP+ cells compared with pellets from passage 2 GFP+ cells, normalizing to DNA content showed that GAG synthesis per cell was highest in pellets from passage 2 GFP+ cells (Fig. 3*C*).

Cartilage-Specific Collagen in Pellets from Passage 2 GFP+ Cells. To further investigate the extracellular matrix components produced by passage 2 GFP+ and passage 2 GFP− cells in pellet culture, we performed immunohistochemical staining for different types of collagen. Cartilage-specific type II collagen and type VI collagen were abundantly produced throughout the pellets from GFP+ cells, but were only present in the periphery of pellets from GFP− cells (Fig. 4*A*). Pellets from GFP− cells showed significant staining for type I collagen in the matrix, whereas pellets from GFP+ cells showed only pericellular staining (Fig. 4*A*). Pellets from both groups of cells showed little staining for type X collagen. Controls confirmed specific antibody staining (Fig. S3). The amount of type I and type II collagen produced in pellets formed using GFP+ cells or GFP− cells (passages 1–3) were quantified using ELISA. Pellets formed with GFP+ cells showed significantly more type II collagen content than the corresponding pellets from GFP− cells at each passage, and the total type II collagen produced by GFP+ cells decreased with passage (Fig. 4*B*). When normalized to DNA content, the maximal production of type II collagen per cell was in pellets from passage 2 GFP+ cells (Fig. 4*B*). Type I collagen content was higher in pellets from passage 1 GFP− cells compared with passage 1 GFP+ cells. With additional passaging in monolayer, the GFP+ cells produced more type I collagen in pellet culture whereas the GFP− cells produced less type I collagen after further expansion (Fig. 4*B*).

Elastic Modulus and Collagen Alignment Vary by Region. To measure the stiffness of matrix produced by cells in pellet culture, microscale elastic moduli were determined using atomic force microscopy (AFM) (Fig. 5). When tested in bulk, pellets from passage 2 GFP+ cells demonstrated a trend toward a higher elastic modulus compared with pellets from passage 2 GFP− cells (20.3 ± 6.3 kPa vs. 11.0 ± 1.9 kPa, $P = 0.14$). Regional elastic modulus was then assessed on cryosections, showing a significantly higher elastic modulus in the region containing the outer 40 μm compared with the region 100–300 μm from the edge of pellets, regardless of whether pellets were formed with GFP+ or GFP− cells. Whereas there was no difference between pellets from GFP+ and GFP− cells in the outer region (25.9 ± 3.2 kPa vs. 25.2 ± 2.4 kPa, $P = 0.97$), the inner region of pellets from GFP+ cells had a significantly higher elastic modulus than the inner region of pellets from GFP− cells (5.8 ± 0.7 kPa vs. 3.6 ± 0.4 kPa, $P < 0.01$). Similar trends were seen when analyzing AFM data for structural indentation stiffness (Fig. S4). Assessment with polarized light showed that the outer region had greater collagen alignment compared with the inner region, and there was a significant correlation of elastic modulus with collagen alignment for both GFP+ ($R^2 = 0.70$, $P < 0.0001$) and GFP− pellets ($R^2 = 0.43$, $P < 0.01$) (Fig. 5*E*).

In Vitro Cartilage Defect Repair with Cells Embedded in Agarose. An in vitro cartilage defect model was established to investigate the ability of iPSC-derived cells to contribute to defect repair. After 21 d of culture in 1% agarose, both passage 3 GFP+ and GFP− cells showed cartilaginous matrix production and integration with the surrounding explant cartilage as determined by histology (Fig. 6*A*). The integrative repair strength was calculated as the peak shear stress at failure as constructs containing GFP+ or GFP− cells were pushed out of the surrounding cartilage explant. This repair strength was significantly higher than that of controls using agarose alone or cored cartilage to fill the defect (Fig. 6*B*). Constructs with GFP+ cells showed significantly higher integrative strength compared with constructs with GFP− cells (48.8 ± 4.9 kPa vs. 29.1 ± 7.6 kPa, $P < 0.01$).

Discussion

Our findings show that, with appropriate differentiation and purification protocols, murine iPSCs can be induced to a chondrogenic lineage characterized by high production of cartilage-

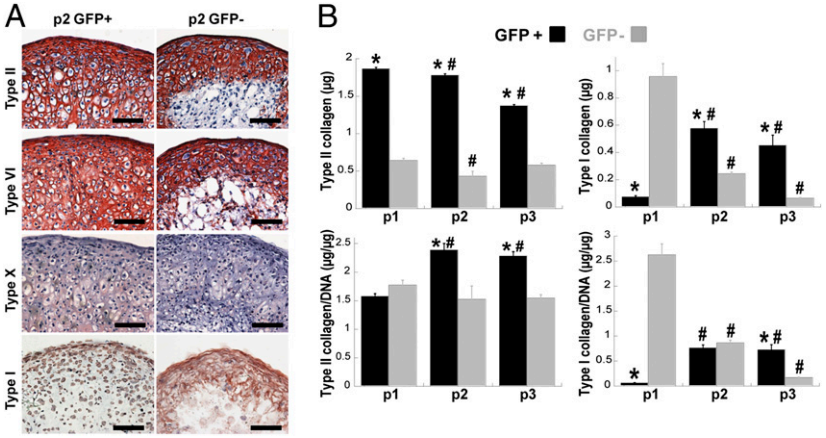

Fig. 4. Collagen production. (*A*) Immunohistochemistry for type II, type VI, type X, and type I collagen (as labeled). (Scale bar: 100 μm.) (*B*) Quantification of type II (*Left*) or type I collagen (*Right*) by ELISA, presented as total content or normalized to DNA content. Asterisk indicates $P < 0.05$ to GFP− of same passage and pound indicates $P < 0.05$ to passage 1 of own cell type, $n \geq 4$ per group, mean ± SEM.

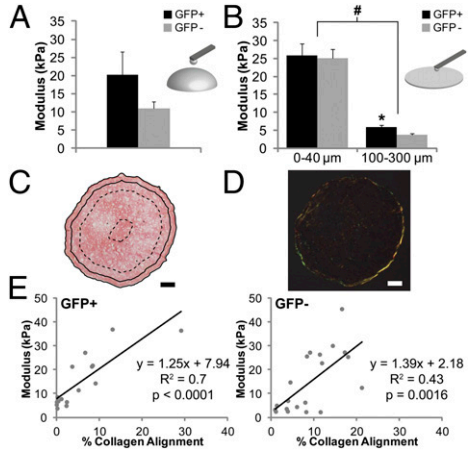

Fig. 5. Mechanical characterization of pellets via AFM. (*A*) Bulk elastic modulus measurements of GFP+ and GFP− pellets, $n \geq 5$, mean ± SEM. (*B*) Regional elastic modulus values from cryosections, $n \geq 4$, mean ± SEM, pound symbol indicates $P < 0.05$ by region and asterisk indicates $P < 0.05$ by cell type. (*C*) Picrosirius red stained section of GFP+ pellet depicting regions tested: 0–40 μm (between solid lines) and 100–300 μm (between dashed lines). (Scale bars: 100 μm.) (*D*) Polarized light micrograph of section in *C*. (*E*) Correlation between regional elastic modulus values and percent collagen alignment within those regions for pellets from GFP+ (*Left*) and GFP− (*Right*) cells.

specific matrix at the gene and protein levels. Using these cells, we sought to produce cartilage tissue-engineered constructs to establish a model system that harnesses the power of mouse genetics for in vitro studies of cartilage injury and repair. We observed the most robust chondrogenic differentiation in this system by using BMP-4 treatment in micromass culture, isolating differentiated cells by Col2 expression, expanding these cells for several passages with bFGF, and subsequently forming pellets that were maintained for 21 d in the presence of TGF-β3. This multistage approach enabled us to generate constructs with high levels of GAG and type II collagen production. Finally, we showed that the iPSC-derived cells were effective at promoting the integration of nascent tissue with the surrounding adult cartilage using an in vitro model of cartilage injury.

There are several advantages to using iPSCs for developing cartilage model systems. These cells can be expanded indefinitely in an undifferentiated state, enabling the derivation of adequate numbers of differentiated progeny for high-throughput analysis and drug screening. In contrast, most adult stem cells such as MSCs and ASCs show changes in differentiation potential after ∼4 passages in culture (33). Derivation of iPSCs from minimally invasive sources such as skin fibroblasts or from joint cells during surgery allows for patient-matched engineered tissues even from elderly patients or those with OA (28, 31). Recent work has shown that iPSCs from patients with complex, polygenic diseases such as sporadic Alzheimer's disease were able to recapitulate the functional deficit of neuronal cells (16), opening up the possibility that iPSC-derived cartilage from patients with OA may show enhanced degradation and aid investigation of OA risk factors and potential treatments. Similarly, generating tissue models from knockout mice that are either susceptible to OA or are protected from OA may allow for mechanistic investigations that are challenging to perform in animal models.

The differentiation of pluripotent cells toward the chondrogenic lineage is a complex process that typically involves multiple steps. For example, Oldershaw and colleagues developed a protocol involving temporally-varied plating densities, matrix substrates, and growth factors to achieve a high percentage of chondrocyte-like cells from human embryonic stem cells (34). Similarly, several studies using mouse or human iPSCs have used 3D embryoid bodies as an intermediate step leading to subsequent chondrogenic differentiation (28–30). We determined that short-term exposure to BMP-4 in serum-free micromass cultures was effective at initiating chondrogenesis. For the second phase of differentiation, cells were grown as pellets in the presence of TGF-β3 to promote matrix formation without the terminal hypertrophic or osteogenic differentiation that can occur with long-term BMP stimulation (35). Additionally, this work extended the concept of multistage chondrogenic differentiation of pluripotent cells by including a purification step to isolate cells that had successfully differentiated toward the chondrogenic lineage.

To efficiently derive a cell source with sufficient chondrogenic capacity, we developed a protocol to isolate subpopulations of cells at the end of micromass culture based on GFP expression under the control of a previously described cartilage-specific Col2 regulatory element (32). This approach allowed us to demonstrate the significance of starting cell population homogeneity in recreating tissues with cartilage-specific physiological properties. The GFP+ (successfully predifferentiated) and GFP− cells (not successfully predifferentiated) showed clear differences in morphology, proliferation rate, and gene expression in monolayer culture, indicating that the sorting procedure generated distinct and well-defined starting cell populations. Pellets formed using GFP+ or GFP− cells confirmed these observations, as GFP+ cells produced larger pellets with increased production of cartilage matrix consisting of sulfated GAGs and type II collagen. Sorting for GFP+ cells not only enhanced the chondrogenic properties of the engineered tissue constructs, but also served to eliminate undifferentiated cells that could potentially form teratomas upon transplantation. The benefit of using a defined starting cell population for iPSC-based therapeutic applications was recently demonstrated in a study showing that positive sorting for a cardiovascular progenitor marker not only encouraged cardiac repair in vivo, but also eliminated the teratoma formation associated with contaminating undifferentiated cells (18).

Continuous passaging of the sorted cells in monolayer culture had an effect on the cell phenotype, with a reduction in Col2 and Acan gene expression along with increased Col1 expression. This result was expected, as human and mouse primary chondrocytes have been previously shown to rapidly undergo a transition to dedifferentiated chondrocytes in culture (36, 37). Contrary to the expectation that matrix synthesis would also decrease with passage, the pellets formed from passage 2 GFP+ cells showed a more uniform distribution of GAG staining and higher synthesis of GAG and type II collagen per cell than passage 1 GFP+ cells. This observation could be due to a preferential expansion of a specific subset within the GFP+ cells during culture with bFGF, as this growth factor has been previously shown to enhance the proliferation and chondrogenic capacity of MSCs (33) and the

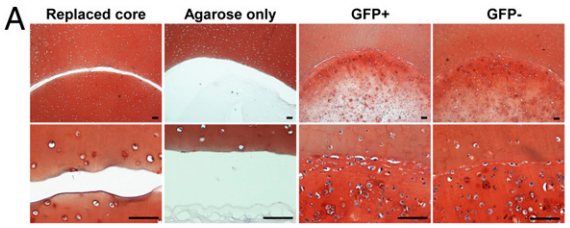

Fig. 6. In vitro cartilage defect repair. (*A*) Cored cartilage explants filled with agarose only, GFP+ cells in agarose, GFP− cells in agarose, or replaced cartilage (as labeled). (Scale bars: 100 μm.) (*B*) Shear strength of repair by the maximum stress as the inner core is pushed out of the explant, $n \geq 5$ per group, mean ± SEM, asterisk indicates $P < 0.05$ to cartilage, pound indicates $P < 0.05$ to agarose, and ampersand indicates $P < 0.05$.

proliferation of iPSC-derived MSC-like cells (30). However, it is important to note that GFP+ cells lost the ability to form homogeneous cartilaginous pellets after being passaged three times, suggesting that whereas limited passaging may prime or preferentially expand cells with the most chondrogenic potential, extensive expansion may lead to dedifferentiation that limits the chondrogenic capacity of the cells.

The specific matrix composition gives an indication of how well the iPSC-derived tissue engineered constructs can serve as an in vitro model for cartilage. Pellets formed using passage 2 GFP+ cells demonstrated robust production of hyaline cartilage-specific type II collagen, and were generally negative for the hypertrophic chondrocyte marker type X collagen and the fibrous tissue marker type I collagen. The lack of a hypertrophic chondrocyte phenotype was particularly interesting as this conversion has been previously reported to occur during chondrogenesis with adult stem cells (38). The avoidance of type I collagen production in pellets from GFP+ cells is an important observation, as the formation of mechanically inferior fibrocartilage instead of hyaline cartilage is associated with the failure of the reparative process in joints (39). Due to the high cellularity of the pellets, staining for type VI collagen was present throughout the matrix, consistent with young cartilage, whereas this protein is typically localized to the pericellular matrix in mature cartilage (40). Taken together, the positive staining of collagen II and VI and the lack of collagen I and X indicate that the iPSC-derived pellets after 21 d of culture are similar to an immature cartilaginous tissue.

As cartilage primarily serves the biomechanical role of distributing forces during joint loading, the ability to assess the mechanical properties of tissue-engineered cartilage is critical (2). In this study, we adapted an AFM-based elastic modulus mapping technique (41) to investigate the intrinsic mechanical properties of cartilaginous matrix synthesized by iPSCs in pellet culture. With the development of a system to match particular genetic profiles to changes in mechanical properties, this approach provides a tool to investigate questions related to cartilage mechanics and mechanotransduction. Microscale testing of cryosections also allows for the assessment of regional variation in elastic moduli. Both GFP+ and GFP− cells synthesized matrix with similar mechanical properties at the periphery of the pellet, but GFP+ cells produced matrix with higher elastic modulus in the central region of the pellet. This finding emphasizes that selecting for the successfully predifferentiated cells enhances the distribution of cartilaginous matrix throughout the construct. Interestingly, the most prominent effect was the greater elastic modulus in the periphery (outer 40 μm) compared with central regions (100–300 μm from the edge) of the pellets. The elastic moduli correlated to collagen alignment, with the stiffer outer region of the pellets showing a higher degree of collagen alignment compared with the central region. This observation is similar to zonal alterations seen in the microscale mechanical properties of native cartilage, with the superficial layer showing a high modulus due to an increased ratio of aligned collagen molecules to GAGs in this zone (42). These results indicate that the engineered cartilage has some of the features of native cartilage architecture, which may be critical to success in defect repair and developing in vitro models to study cartilage biology and mechanics.

Autologous chondrocyte implantation (ACI) is the only cell-based treatment that is FDA-approved for treating focal cartilage defects (Carticel, Genzyme Biosurgery). An important step in evaluating novel cell sources for defect repair is to demonstrate integration of newly developing tissue with native cartilage, as the synthesis of matrix by cells can affect the strength of cartilage integration (43–45). We found that sorted and expanded iPSC-derived cells seeded in agarose were effective at filling the defect with cartilaginous matrix that integrated well with the surrounding cartilage. Interestingly, matrix production by iPSCs was enhanced near the native cartilage surface, possibly due to paracrine signals from chondrocytes (46). The agarose constructs with cells contributed to a defect repair that far exceeded native cartilage healing and the cell-free agarose group, which provides a control for the effects of friction. Constructs made with GFP+ cells showed the highest integrative repair strength, further confirming the utility of using predifferentiation and cell purification to enhance the therapeutic potential of iPSC-derived cell populations for cartilage defect repair.

This study provides a proof-of-principle strategy for using iPSCs as a cell source for cartilage tissue engineering. The ability to derive large numbers of cells with chondrogenic potential from a noninvasively isolated somatic cell starting population is an important advance for the development of cellular therapy strategies to treat osteoarthritis. Additionally, we used techniques to purify a defined cell population with enhanced chondrogenic potential from undifferentiated and off-target cell types, providing a pathway for maximizing therapeutic effectiveness while minimizing the risk of teratoma formation. Finally, this work also establishes a tool for performing mechanistic in vitro studies using iPSCs from mouse strains with unique phenotypes related to cartilage development, repair, and osteoarthritis.

Materials and Methods

Induced Pluripotent Stem Cell Derivation and Culture. All procedures were performed in accordance with a protocol approved by the Duke University Institutional Animal Care and Use Committee. The details of tail fibroblast isolation from 8- to 10-wk-old mice and derivation of iPSCs can be found in *SI Materials and Methods*. Briefly, reprogramming was performed by transducing tail fibroblasts with a single doxycycline-inducible lentiviral vector controlling the transgenic expression of mouse cDNAs for Oct4 (Pou5f1), Sox2, Klf4, and c-Myc (47) for 24 h. After ~2 wk, individual colonies were manually selected based on morphology and colonies were maintained on feeder cells in iPSC media without doxycycline. Nucleofection with Col2-GFP plasmid (32) and selection with G418 generated clones that were further screened based on the specific increase in GFP+ expression after chondrogenic induction in micromass culture.

Micromass Culture and Cell Sorting. Reagents from Sigma-Aldrich unless noted. Feeder cells were removed using two subtraction steps of 45 min on tissue culture plastic separated by a day of culture on 0.1% gelatin. Cells were resuspended at a concentration of 2×10^7 cells/mL, and micromasses were established by plating 2×10^5 iPSCs in 10 μl into individual wells of 48 well plates (Corning) or 30 micromasses in a 10 cm dish (BD). After 2–3 h incubation, additional iPSC medium with 10% serum without LIF was added. The following day, media was switched to serum-free chondrogenic differentiation medium containing DMEM-HG, NEAA, 2-me, ITS+ premix (BD), penicillin-streptomycin (P/S, Gibco), 50 μg/mL L-ascorbic acid 2-phosphate, and 40 μg/mL L-proline. Micromasses were cultured for 15 d, with 50 ng/mL mBMP-4 (R&D Systems) and 100 nM dexamethasone added to the chondrogenic medium during days 3–5 of culture only. Micromasses were then digested for 1 h using 0.4% collagenase type II (Worthington), 1320 PKU/mL pronase (Calbiochem), and 10 μg/mL DNase I (Worthington). Cells were centrifuged, incubated with 0.25% tryspin-EDTA for 5 min, and resuspended in sort medium containing DMEM-HG, 2% FBS, DNase I, 10 mM Hepes (Gibco), 2× P/S/F, and 5 μM propidium iodide (Biolegend). Cells were sorted based on GFP expression using the 100 μM nozzle of a Cytomation MoFlo sorter (Beckman Coulter). Cells designated as "unsorted" were plated directly after micromass digestion.

Cell Expansion and Pellet Culture. Cells sorted as GFP− or GFP+ were plated at 1×10^4 cells per cm^2 on gelatin coated plates in chondrogenic differentiation medium with the addition of 10% FBS and 4 ng/mL bFGF (Roche). Cells were passaged upon subconfluence every 2–3 d using 0.05% trypsin-EDTA (Sigma-Aldrich). Pellets were formed by centrifuging 2.5×10^5 cells at $200 \times g$ for 5 min in 15-mL tubes. Pellets were cultured in chondrogenic differentiation medium containing 10 ng/mL TGF-β3 (R&D Systems) and 100 nM dexamethasone for 21 d.

Analysis of Pluripotency and Karyotype. Detailed methods can be found in *SI Materials and Methods*. Teratoma formation and karyotype analysis were performed by Applied Stem Cell.

Immunocytochemistry, RT-PCR, Histology, and Immunohistochemistry. Detailed methods can be found in *SI Materials and Methods*.

Biochemical Analysis. Some pellets were digested using pepsin and elastase at 4 °C and analyzed for type I and type II collagen using ELISA kits according to the manufacturer's protocol (Chondrex). Digested samples were also analyzed for glycosaminoglycans (GAGs) and dsDNA as described (48).

Atomic Force Microscopy. Pellets were mechanically tested using an atomic force microscope to determine bulk and regionally varying elastic moduli using techniques based on previous work (41) as described in detail in *SI Materials and Methods*.

Collagen Alignment. Cryosections from each pellet were stained with Picrosirius red and imaged under polarized light to assess collagen alignment as described in detail in *SI Materials and Methods*.

Cartilage Defect Repair Assay. Cartilage explants of 5 mm diameter were taken from healthy areas of the femoral cartilage of young pigs and kept in chondrogenic differentiation medium containing 10% FBS. Explants were then cored using a 3 mm biopsy punch and immobilized on a thin layer of molten 2% agarose that was allowed to cool. Passage 3 GFP+ or GFP− cells in chondrogenic differentiation media were mixed 1:1 with 2% agarose for delivery to the defect area with a final concentration of 1×10^6 cells in 10 μL of 1% agarose. Filling the defect area with agarose alone or immediately replacing the 3 mm cartilage core served as controls. Samples were cultured for 21 d with chondrogenic differentiation medium containing 10 ng/mL TGF-β3 and 100 nM dexamethasone. After 21 d, samples were processed for histology ($n = 2$ per group) or used to assess the mechanical strength of the defect repair ($n \geq 5$ per group) by measuring the peak shear stress during a push-out test in a size-adjusted version of a described method (49).

Statistical Analysis. Statistical analysis was performed using a *t* test or analysis of variance (ANOVA) with $\alpha = 0.05$ as described in *SI Materials and Methods*.

ACKNOWLEDGMENTS. We thank Dr. William Horton of Portland Shriners Research Center for providing the Col2-GFP construct, Nancy Martin of the Flow Cytometry Shared Resource, as well as Shannon O'Connor, Syandan Chakraborty, and Malathi Chellappan for their contributions. Funding from National Institutes of Health Grants AR50245, AR48852, AG15768, and AR48182, and Training Grant T32AI007217 (to V.P.W.); a National Science Foundation Graduate Research Fellowship (to B.O.D.); a Pratt School of Engineering Undergraduate Fellowship (to H.S.); the AO Foundation; the AOSpine Foundation; and the Arthritis Foundation.

1. Hunziker EB (2002) Articular cartilage repair: Basic science and clinical progress. A review of the current status and prospects. *Osteoarthritis Cartilage* 10(6):432–463.
2. Guilak F, Butler DL, Goldstein SA (2001) Functional tissue engineering: the role of biomechanics in articular cartilage repair. *Clin Orthop Relat Res* (391, Suppl): S295–S305.
3. Song L, Baksh D, Tuan RS (2004) Mesenchymal stem cell-based cartilage tissue engineering: cells, scaffold and biology. *Cytotherapy* 6(6):596–601.
4. Brittberg M, et al. (1994) Treatment of deep cartilage defects in the knee with autologous chondrocyte transplantation. *N Engl J Med* 331(14):889–895.
5. Lee CR, Grodzinsky AJ, Hsu HP, Martin SD, Spector M (2000) Effects of harvest and selected cartilage repair procedures on the physical and biochemical properties of articular cartilage in the canine knee. *J Orthop Res* 18(5):790–799.
6. Guilak F, Estes BT, Diekman BO, Moutos FT, Gimble JM (2010) 2010 Nicolas Andry Award: Multipotent adult stem cells from adipose tissue for musculoskeletal tissue engineering. *Clin Orthop Relat Res* 468(9):2530–2540.
7. Nöth U, Steinert AF, Tuan RS (2008) Technology insight: Adult mesenchymal stem cells for osteoarthritis therapy. *Nat Clin Pract Rheumatol* 4(7):371–380.
8. Pittenger MF, et al. (1999) Multilineage potential of adult human mesenchymal stem cells. *Science* 284(5411):143–147.
9. Diekman BO, Rowland CR, Lennon DP, Caplan AI, Guilak F (2010) Chondrogenesis of adult stem cells from adipose tissue and bone marrow: Induction by growth factors and cartilage-derived matrix. *Tissue Eng Part A* 16(2):523–533.
10. Dexheimer V, Mueller S, Braatz F, Richter W (2011) Reduced reactivation from dormancy but maintained lineage choice of human mesenchymal stem cells with donor age. *PLoS ONE* 6(8):e22980.
11. Murphy JM, et al. (2002) Reduced chondrogenic and adipogenic activity of mesenchymal stem cells from patients with advanced osteoarthritis. *Arthritis Rheum* 46(3):704–713.
12. Takahashi K, et al. (2007) Induction of pluripotent stem cells from adult human fibroblasts by defined factors. *Cell* 131(5):861–872.
13. Takahashi K, Yamanaka S (2006) Induction of pluripotent stem cells from mouse embryonic and adult fibroblast cultures by defined factors. *Cell* 126(4):663–676.
14. Yu J, et al. (2007) Induced pluripotent stem cell lines derived from human somatic cells. *Science* 318(5858):1917–1920.
15. Park IH, et al. (2008) Disease-specific induced pluripotent stem cells. *Cell* 134(5):877–886.
16. Israel MA, et al. (2012) Probing sporadic and familial Alzheimer's disease using induced pluripotent stem cells. *Nature* 482(7384):216–220.
17. Yoshida Y, Yamanaka S (2010) Recent stem cell advances: Induced pluripotent stem cells for disease modeling and stem cell-based regeneration. *Circulation* 122(1):80–87.
18. Blin G, et al. (2010) A purified population of multipotent cardiovascular progenitors derived from primate pluripotent stem cells engrafts in postmyocardial infarcted nonhuman primates. *J Clin Invest* 120(4):1125–1139.
19. Kramer J, et al. (2000) Embryonic stem cell-derived chondrogenic differentiation in vitro: Activation by BMP-2 and BMP-4. *Mech Dev* 92(2):193–205.
20. Nakayama N, Duryea D, Manoukian R, Chow G, Han CY (2003) Macroscopic cartilage formation with embryonic stem-cell-derived mesodermal progenitor cells. *J Cell Sci* 116(Pt 10):2015–2028.
21. Hwang NS, et al. (2006) Effects of three-dimensional culture and growth factors on the chondrogenic differentiation of murine embryonic stem cells. *Stem Cells* 24(2):284–291.
22. Koay EJ, Hoben GM, Athanasiou KA (2007) Tissue engineering with chondrogenically differentiated human embryonic stem cells. *Stem Cells* 25(9):2183–2190.
23. Toh WS, et al. (2007) Effects of culture conditions and bone morphogenetic protein 2 on extent of chondrogenesis from human embryonic stem cells. *Stem Cells* 25(4):950–960.
24. Yamashita A, Nishikawa S, Rancourt DE (2010) Identification of five developmental processes during chondrogenic differentiation of embryonic stem cells. *PLoS ONE* 5(6):e10998.
25. Gong G, Ferrari D, Dealy CN, Kosher RA (2010) Direct and progressive differentiation of human embryonic stem cells into the chondrogenic lineage. *J Cell Physiol* 224(3): 664–671.
26. Nakagawa T, Lee SY, Reddi AH (2009) Induction of chondrogenesis from human embryonic stem cells without embryoid body formation by bone morphogenetic protein 7 and transforming growth factor beta1. *Arthritis Rheum* 60(12):3686–3692.
27. Hwang NS, Varghese S, Zhang Z, Elisseeff J (2006) Chondrogenic differentiation of human embryonic stem cell-derived cells in arginine-glycine-aspartate-modified hydrogels. *Tissue Eng* 12(9):2695–2706.
28. Kim MJ, et al. (2011) Generation of human induced pluripotent stem cells from osteoarthritis patient-derived synovial cells. *Arthritis Rheum* 63(10):3010–3021.
29. Medvedev SP, et al. (2011) Human induced pluripotent stem cells derived from fetal neural stem cells successfully undergo directed differentiation into cartilage. *Stem Cells Dev* 20(6):1099–1112.
30. Teramura T, et al. (2010) Induction of mesenchymal progenitor cells with chondrogenic property from mouse-induced pluripotent stem cells. *Cell Reprogram* 12(3):249–261.
31. Wei Y, et al. (2012) Chondrogenic differentiation of induced pluripotent stem cells from osteoarthritic chondrocytes in alginate matrix. *Eur Cell Mater* 23:1–12.
32. Grant TD, et al. (2000) Col2-GFP reporter marks chondrocyte lineage and chondrogenesis during mouse skeletal development. *Dev Dyn* 218(2):394–400.
33. Solchaga LA, Penick K, Goldberg VM, Caplan AI, Welter JF (2010) Fibroblast growth factor-2 enhances proliferation and delays loss of chondrogenic potential in human adult bone-marrow-derived mesenchymal stem cells. *Tissue Eng Part A* 16(3):1009–1019.
34. Oldershaw RA, et al. (2010) Directed differentiation of human embryonic stem cells toward chondrocytes. *Nat Biotechnol* 28(11):1187–1194.
35. Hellingman CA, et al. (2011) Smad signaling determines chondrogenic differentiation of bone-marrow-derived mesenchymal stem cells: Inhibition of Smad1/5/8P prevents terminal differentiation and calcification. *Tissue Eng Part A* 17(7-8):1157–1167.
36. Darling EM, Athanasiou KA (2005) Rapid phenotypic changes in passaged articular chondrocyte subpopulations. *J Orthop Res* 23(2):425–432.
37. Gosset M, Berenbaum F, Thirion S, Jacques C (2008) Primary culture and phenotyping of murine chondrocytes. *Nat Protoc* 3(8):1253–1260.
38. Dickhut A, et al. (2009) Calcification or dedifferentiation: Requirement to lock mesenchymal stem cells in a desired differentiation stage. *J Cell Physiol* 219(1):219–226.
39. Kreuz PC, et al. (2006) Results after microfracture of full-thickness chondral defects in different compartments in the knee. *Osteoarthritis Cartilage* 14(11):1119–1125.
40. Alexopoulos LG, Youn I, Bonaldo P, Guilak F (2009) Developmental and osteoarthritic changes in Col6a1-knockout mice: Biomechanics of type VI collagen in the cartilage pericellular matrix. *Arthritis Rheum* 60(3):771–779.
41. Darling EM, Wilusz RE, Bolognesi MP, Zauscher S, Guilak F (2010) Spatial mapping of the biomechanical properties of the pericellular matrix of articular cartilage measured in situ via atomic force microscopy. *Biophys J* 98(12):2848–2856.
42. Wilusz RE, Defrate LE, Guilak F (2012) Immunofluorescence-guided atomic force microscopy to measure the micromechanical properties of the pericellular matrix of porcine articular cartilage. *J R Soc Interface* 9(76):2997–3007.
43. Giurea A, DiMicco MA, Akeson WH, Sah RL (2002) Development-associated differences in integrative cartilage repair: roles of biosynthesis and matrix. *J Orthop Res* 20(6):1274–1281.
44. Obradovic B, et al. (2001) Integration of engineered cartilage. *J Orthop Res* 19(6):1089–1097.
45. Reindel ES, et al. (1995) Integrative repair of articular cartilage in vitro: Adhesive strength of the interface region. *J Orthop Res* 13(5):751–760.
46. Liu X, et al. (2010) In vivo ectopic chondrogenesis of BMSCs directed by mature chondrocytes. *Biomaterials* 31(36):9406–9414.
47. Carey BW, et al. (2009) Reprogramming of murine and human somatic cells using a single polycistronic vector. *Proc Natl Acad Sci USA* 106(1):157–162.
48. Estes BT, Diekman BO, Gimble JM, Guilak F (2010) Isolation of adipose-derived stem cells and their induction to a chondrogenic phenotype. *Nat Protoc* 5(7):1294–1311.
49. Hennerbichler A, Moutos FT, Hennerbichler D, Weinberg JB, Guilak F (2007) Repair response of the inner and outer regions of the porcine meniscus in vitro. *Am J Sports Med* 35(5):754–762.